World Academy of Science, Engineering and Technology
International Journal of Nuclear and Quantum Engineering
Vol:15, No:10, 2021

Neural Network Supervisory Proportional-Integral-Derivative Control of the Pressurized Water Reactor Core Power Load Following Operation

Derjew Ayele Ejigu, Houde Song, Xiaojing Liu

***Abstract*—**This work presents the particle swarm optimization trained neural network (PSO-NN) supervisory proportional integral derivative (PID) control method to monitor the pressurized water reactor (PWR) core power for safe operation. The proposed control approach is implemented on the transfer function of the PWR core, which is computed from the state-space model. The PWR core state-space model is designed from the neutronics, thermal-hydraulics, and reactivity models using perturbation around the equilibrium value. The proposed control approach computes the control rod speed to maneuver the core power to track the reference in a closed-loop scheme. The particle swarm optimization (PSO) algorithm is used to train the neural network (NN) and to tune the PID simultaneously. The controller performance is examined using integral absolute error, integral time absolute error, integral square error, and integral time square error functions, and the stability of the system is analyzed by using the Bode diagram. The simulation results indicated that the controller shows satisfactory performance to control and track the load power effectively and smoothly as compared to the PSO-PID control technique. This study will give benefit to design a supervisory controller for nuclear engineering research fields for control application.

***Keywords*—**Machine learning, neural network, pressurized water reactor, supervisory controller.

I. Introduction

THE pressurized water reactor (PWR) is a complex system that uses water as a coolant and a moderator. The parameters of the PWR are dynamic and vary with power level as a function of time. Thus, the mathematical equations are developed based on assumptions and therefore do not represent the actual PWR model. Consequently, the PWR faces uncertainties and needs a controller for safety operation. Different control approaches including traditional PID and intelligent controllers are applied to regulate the PWR power.

The proportional-integral-derivative (PID) controller is commonly used in most industrial processes [1]. In the case of nuclear engineering, the PID controller is applied to monitor the core output power [2]-[4]. PID is also used to control the steam generator water level of PWR [5]. However, the tuning of the PID parameters is a difficult task and time-consuming using traditional, and trial and error methods. Hence, the PID controller is unable to handle the data and shows overshoot and undershoot. Thus, the drawbacks of the PID controller could be overcome by using population-based algorithms and artificial neural network approaches.

The artificial neural network (ANN) is a machine learning technique applied to control load following operation of a nuclear reactor [6], [7], to identify nuclear reactor black box model [8], to control the feedwater of a steam generator [9], to predict the moderator temperature of the heavy water reactor, and the core parameter of PWR [10], [11], to diagnose the transients of a nuclear power plant [12], to handle large nuclear reactor data, make decisions, predict, and control [13], and others.

The ANN could be trained by using different algorithms, and gradient descent is the common method [14]. However, the gradient descent method gives the optimal model without training the whole dataset. This shortcoming can be overcome by using a population-based iterative intelligent algorithm.

The population-based algorithms are currently applied to train ANN to solve different complex problems in various research areas. Particle swarm optimization (PSO) algorithm is applied to train ANN [15]-[17] and tune the PID parameters automatically for control application [18], [19].

The ANN is also used to supervise other control methods to ensure effective, optimal, and stable control action in different research areas, including nuclear engineering [20]-[24].

The drawbacks of the PID in data handling, controlling, and optimization could be overcome by supervising using intelligent algorithms. This work proposes the PSO-NN supervisory PID control approach to monitor the PWR core power for load following application in a closed-loop scheme. This control method is simple to implement on any dynamic system for stable control action and reference tracking. The rest of this paper first explains the methodology, which includes the state-space model of PWR core and the proposed control method. Then followed by detailed results and conclusion.

II. PWR Core Model

The PWR core model is designed from the neutronics, thermal-hydraulics, and reactivity models. The neutronics model describes the time domain of the neutron population and the power in the reactor core region. The neutronics model for one energy group and a single delayed precursor neutron group is mathematically represented as;

Derjew Ayele Ejigu and Houde Song are with the Shanghai Jiao Tong University, China (e-mails: derjew_ayele@ yahoo.com, hdsong@sjtu.edu.cn).
Xiaojing Liu is with the Shanghai Jiao Tong University, China (corresponding author e-mail: xiaojingliu@sjtu.edu.cn).

The authors sincerely acknowledge the financial support of National Natural Science Foundation of China (Grant number: 11922505).

$$dn/dt = [(\rho - \beta)/\tau] + \lambda c \quad (1)$$

$$dc/dt = (\beta/\tau)n - \lambda c \quad (2)$$

where, n, c, ρ, β, τ, and λ are the neutron density, delayed neutron precursor concentration, total reactivity, delayed neutron fraction, prompt neutron lifetime, and delayed neutron decay constant respectively.

The thermal-hydraulics model is used to compute the heat transfer process in a nuclear reactor. This model is designed from a single fuel temperature and the average temperature of two coolant temperature regions based on Mann's formulation [25] as shown in Fig. 1. The model complexities are avoided by considering assumptions like one-dimensional fluid flow, well-stirred coolant lumps, and constant heat transfer coefficient from fuel to coolant.

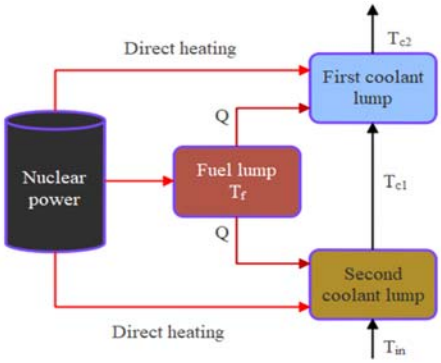

Fig. 1 The heat transfer process

The mathematical expression of the thermal-hydraulics model of the PWR core is designed from a single fuel, and average coolant temperatures, which is given by;

$$dT_f/dt = (f/\mu_f)P - (\Omega/\mu_f)(T_f - T_c) \quad (3)$$

$$dT_c/dt = [(1-f)/2\mu_c]P + (\Omega/2\mu_c)(T_c - T_c) - (M/\mu_c)(T_{c2} - T_{c1} \quad (4)$$

where, T_f, T_{c1}, and T_{c2} are temperatures of the fuel, inlet coolant, and outlet coolant respectively.

The average coolant temperature (T_c) is expressed as;

$$T_c = (T_{c1} + T_{c2})/2 \quad (5)$$

The PWR power (P) is proportional to the neutron density which is given as;

$$P = P_o n \quad (6)$$

where, P_o and n represent the nominal and relative power respectively.

The reactivity term in the neutronics model is the sum of the reactivity changes due to control rod movement, fuel, and moderator temperatures. The total reactivity is given by;

$$\rho = \Delta\rho_r + \alpha_f \Delta T_f + (\alpha_c/2)\Delta T_{c2} \quad (7)$$

where, α_f, and α_c are the reactivity feedback coefficients of the fuel and coolant respectively. The terms ρ_r and Δ denote the reactivity due to control rod movement and the deviation respectively.

The neutronics, thermal-hydraulics and reactivity models are interdependent with each other. These models could be combined and linearized around the steady-state value using deviations for various purposes such as control design and to describe the behavior of the PWR. The deviations of the point kinetics and thermal-hydraulics model state variables are given as;

$$n = n_o + \Delta n \quad (8)$$

$$c = c_o + \Delta c \quad (9)$$

$$T_f = T_{f,o} + \Delta T_f \quad (10)$$

$$T_{c1} = T_{c1,o} + \Delta T_{c1} \quad (11)$$

$$T_{c2} = T_{c2,o} + \Delta T_{c2} \quad (12)$$

where, $(.)_o$ indicates the equilibrium values.

The rate of change of the state variables of the reactor at steady state is zero. The inlet coolant temperature of PWR is considered as constant and the perturbation is zero. Substitute (5-12) into (1-4), the simplified and linearized PWR core model equations are written as;

$$d\Delta n/dt = (-\beta/\tau)\Delta n + \lambda\Delta c + [(\alpha_f n_o)/\tau]\Delta T_f + [(\alpha_c n_o)/2\tau]\Delta T_{c2} + (n_o/\tau)\Delta\rho_r \quad (13)$$

$$d\Delta c/dt = (\beta/\tau)\Delta n - \lambda\Delta c \quad (14)$$

$$d\Delta T_f/dt = (fP_o/\mu_f)\Delta n - (\Omega/\mu_f)\Delta T_f + (\Omega/2\mu_f)\Delta T_{c2} \quad (15)$$

$$d\Delta T_{c2}/dt = [(1-f)P_o/\mu_c]\Delta n + (\Omega/\mu_c)\Delta T_f - [(2M+\Omega)/\mu_c]\Delta T_{c2} \quad (16)$$

$$d\Delta\rho_r/dt = G_r v_r \quad (17)$$

Equations (13)-(17) could be stated in a simple form called the state-space model. The state-space model of the dynamic system is a set of first-order differential equations used to investigate the inputs and outputs. The output variables are selected from the state variables. The state-space model and the

corresponding output is given by;

$$dx(t)/dt = Ax(t) + Bu(t) \quad (18)$$

$$y(t) = Cx(t) \quad (19)$$

where, *x(t), y(t)*, and *u(t)* are the state output and input variables respectively. The coefficients *A, B* and *C* are the state, input and output matrices respectively.

Equation (18) clearly shows the input and output variables. The control rod movement is the input variable, and the output variable could be selected from the state variables based on the control interest.

In PWR, the coefficients α_f, α_c, μ_c, Ω, and *M* vary as a function of operational power level, and mathematically written as [7], [26], [27].

$$\alpha_f = (n_o - 4.24)\times 10^{-5} \quad (20)$$

$$\alpha_c = (-4n_o - 17.3)\times 10^{-5} \quad (21)$$

$$\mu_c = (160/9)n_o + 54.002 \quad (22)$$

$$\Omega = (5/3)n_o + 4.9333 \quad (23)$$

$$M = 28n_o + 74 \quad (24)$$

Further, the values of the rest constants are given in Table I.

TABLE I
THE CONSTANTS

Constants	Values
P_o	300 MW
β	0.00619
λ	0.1 s^{-1}
τ	0.00002 s
f	0.975
μ_f	26.3 MW.s/°C
G_r	0.002

The state-space model equation given by (18) and (19) represents an open-loop system which can be represented using block diagrams as shown in Fig. 2.

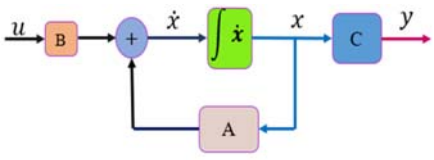

Fig. 2 The block diagram representation of the open-loop state-space model

The system to be controlled is represented using the state-space model and transfer function. The transfer function of an LTI system is calculated from the state space model using Laplace transformation. The transfer function of the PWR model is given by;

$$G(S) = Y(S)/U(S) = C(IS - A)^{-1}B \quad (25)$$

where, *I* and *S* are the identity matrix and the Laplace variable respectively.

The transfer function is then discretized to implement the proposed control approach.

III. PSO-NN Supervisory PID Controller

In control theory, the controller computes the control input to optimize the plant output and track the reference input. The supervisory control method is used to facilitate the decision-making process for effective, stable, and adaptive control action [28]. The PSO-NN supervisory PID control structure is composed of the NN and PID controllers in a closed-loop structure as shown in Fig. 3. The PWR core model output is compared with the reference value to calculate the tracking error. The PWR core output, the control input, and the error are used as input to train the NN using the PSO algorithm. The PSO algorithm is also used to tune the PID parameters. The PID controller filters the error to generate the PID output that is supervised by the NN. Further, the error is fed to the NN to adapt the system to the working environment. The components of the controller are discussed in the following subsections in detail.

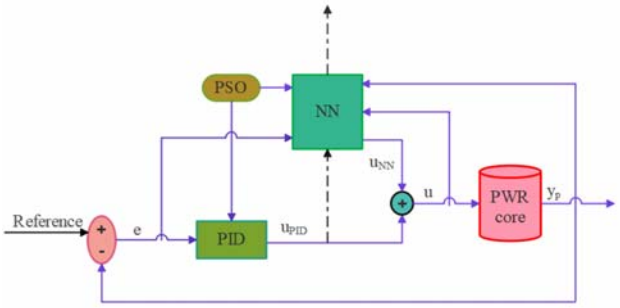

Fig. 3 The control scheme

A. The Neural Network

The NN is an intelligent data computing method that works based functioning human brain. This network is used for system identification, prediction, and control applications from observational data. NN can adapt variable conditions by updating connection weights. The NN consists of a single hidden layer between the input and output layers as depicted in Fig. 4. Each layer consists of different number of neurons depending on the problem type. The connection weights are used to link the neurons of successive layers. The input layer receives the input data, the hidden layer processes the weighted data, and the output layer gives the processed data to users.

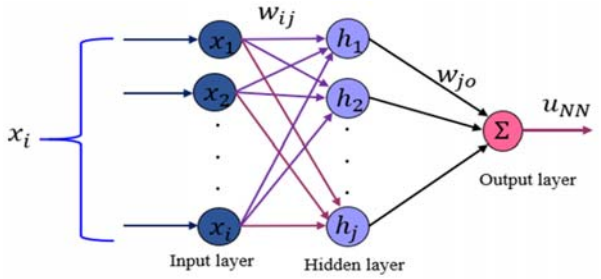

Fig. 4 The NN architecture

The input layer receives the input data, (x_i), and fed weighted data to the hidden layer. The hidden layer contains summation and radial basis activation functions. The summation function sums up the weighted inputs and the activation function process the dataset and introduces nonlinearity to the network. The hidden neurons sum up the weighted inputs, which is given by;

$$p_{ij} = \sum w_{ij} x_i \tag{26}$$

where, $w_{(.)}$ are the connection weight of successive layers.

The radial basis activation function of the hidden neurons processes the summed weighted inputs given by;

$$h_j = \exp(\| p_{ij} - C_n \|^2 / b^2) \tag{27}$$

where, i and j indicate the number of neurons of the input, and hidden layers respectively.

The output layer then receives the weighted values of the processed data and then sends the data to users. The output neuron consists of linear activation function and summation functions. The output of the NN is given by;

$$u_{NN} = \sum_{j=1}^{n} w_{jo} h_j \tag{28}$$

The network propagates forward to train the network using the data in a closed-loop scheme until the proposed learning cycles, called epochs, ends.

B. The PID Controller

The PID controller is a combination of the proportional *(P),* integral (*I*), and derivative *(D)* controllers as shown in Fig. 5. The *P, I*, and *D* terms provide stable operation, limit the speed of the system response, and improves the stability of the system respectively.

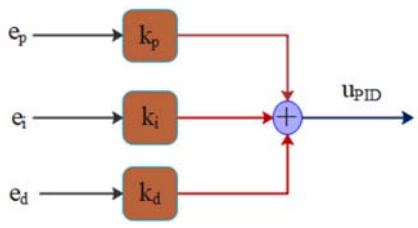

Fig. 5 The PID control structure

The PID controller provides a control signal which is proportional to the tracking error of the system in the past, present, and future. The PID controller output is given by;

$$u_{PID} = k_p e + k_i \int e dt + k_d (de/dt) \tag{29}$$

where, k_p, k_i, and k_d are the proportional, integral, and derivative gains respectively.

The total control input of the PWR core model is the sum of the outputs of the NN and PID controllers. The control input pushes the PWR core output to follow the reference value. The total control input is given by;

$$u = u_{NN} + u_{PID} \tag{30}$$

The PSO algorithm is used to train the NN and tune the PID gains for effective control action.

C. The Particle Swarm Optimization Algorithm

Particle swarm optimization (PSO) is a population-based intelligent algorithm inspired by a group of birds and fishes. The particles move in space randomly and each particle represents a solution to the given optimization problem [15], [29]. The particles are accelerated towards the best position by updating the inertial weights at each iteration. The velocity and position of the swarm in a given dimensional space are given by;

$$\begin{aligned} v_{i,d}(k+1) &= w v_{i,d}(k) + c_1 r_1 [p_{i,d}(k) - x_{i,d}(k)] \\ &+ c_2 r_2 [p_{g,d}(k) - x_{i,d}(k)] \end{aligned} \tag{31}$$

$$x_{i,d}(k+1) = x_{i,d}(k) + v_{i,d}(k+1) \tag{32}$$

where, $v_{i,d}$, $x_{i,d}$, $p_{i,d}$, $p_{g,d}$, and w are the velocity, position, best position, global best position, and inertial weight of the particles respectively. The subscripts i and d represent the number of particles, and the dimension of the search space respectively. Further, r_1 and r_2 are random numbers between [0 1] range, and the constants c_1 and c_2 are the acceleration coefficients in [0 1] interval.

D. The Jacobian and Performance Indices

The effect of the control input on the model output is estimated by using Jacobian. The Jacobian is also used to assess the performance of the NN [30], which is expressed as;

$$\begin{aligned} &\partial y_p / \partial u \approx \partial u_{NN} / \partial u \\ &= (\partial u_{NN} / \partial h_j)(\partial h_j / \partial p_{ij})(\partial p_{ij} / \partial u) \end{aligned} \tag{33}$$

Further, the performance of the controller is evaluated by the integral square error (ISE), integral absolute error (IAE), integral time square error (ITSE), and integral time absolute error (ITAE) criterion functions. These functions are given by;

$$ISE(t) = \int (e(t))^2 dt \quad (34)$$

$$IAE(t) = \int |e(t)| dt \quad (35)$$

$$ITSE(t) = \int t(e(t))^2 dt \quad (36)$$

$$ITAE(t) = \int t|e(t)| dt \quad (37)$$

where, t is the time.

IV. Results

This section presents the simulation results obtained by implementing the proposed control approach on the PWR core model. The simulation is held on the MATLAB environment. The NN has a 3-8-1 orientation, and the connection weights are initialized randomly. The population size was set as 10, and the initial position of the swarm is assigned randomly. The dimension of the swarm position is the same as the network hidden neurons. The controller is trained for 100 iterations.

The PSO-NN supervisory PID control capability is tested on ramp-shaped reference profiles of the PWR power in two control loops.

A. The Power Control Loop-I

The first case considers that the PWR core power load changes as follows: Initially, for 200s the desired fractional full power (FFP) is maintained at 1.0FFP, then reduced to 0.8FFP in 150 s, then held at 0.8FFP for 300 s, and increased to 1.0FFP in 150 s, finally held at 1.0FFP for the rest duration. The performance of the proposed controller with regards to reference tracking and load power controlling is shown in Fig. 6 (a). The PSO-NN effectively supervises the PSO-PID to track the demand power variations successfully as compared with the PSO-PID control approach. Further, the proposed control technique follows the reference value faster than the PSO-PID method when the load power changes. This prevails that the PSO-NN supervisory PID controller is more accurate, and effective than the PSO-PID approach to regulate the core power load change.

The tracking error and the error distributions are depicted in Fig. 6 (b). The controller filters the error and computes the control input of the PWR core model to adjust the output power. The control rod speed computed by both controllers is shown in Fig. 6 (c). The effect of the control rod speed on the PWR output power is measured using the Jacobian value. As shown in Fig. 6 (d), the Jacobian values are small which confirms that the controller filters the error efficiently. Further, the control rod speed is less sensitive to the output power. Fig. 6 (e) illustrates the performance of the controller, measured by ISE, IAE, ITSE, and ITAE criterion functions that decline with iterations. The figure shows that the ITAE function has the highest convergence rate as compared to others. The graph is also used to select the appropriate performance index for fast computational effort and less cost to different control applications.

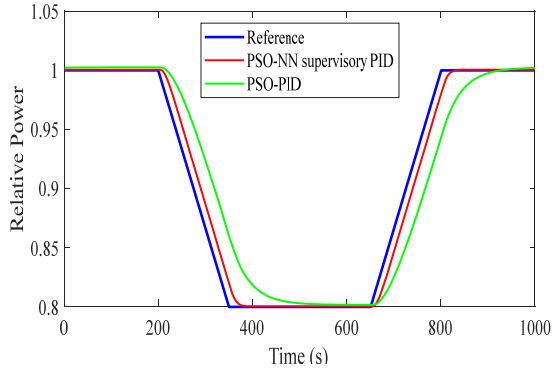

(a) Relative power

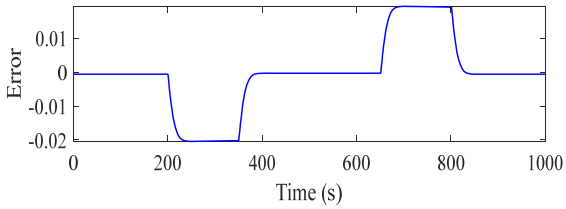

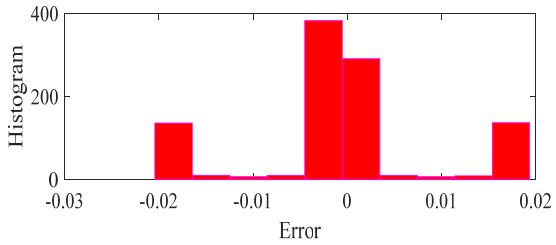

(b) The error and error distribution

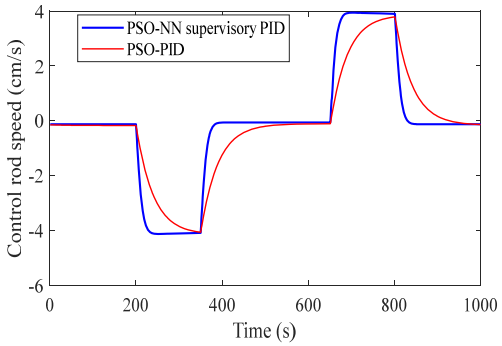

(c) The control input

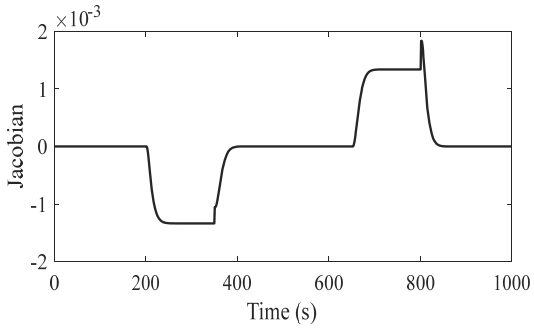

(d) The Jacobian values

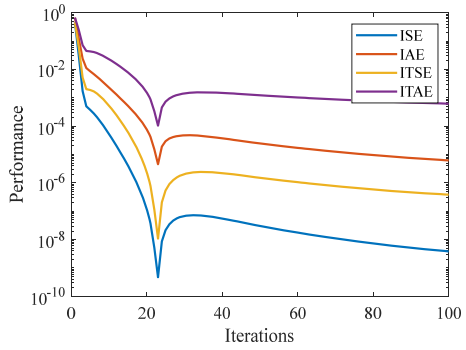

(e) The performance of the controller

Fig. 6 The simulation results

B. The Power Control Loop-2

For the second case, the FFP reference was initially set at 0.4FFP for 100s, then increased to 0.6FFP in 250 s, held at 0.6FFP for 600 s, and decreased to 0.4FFP in 250 s, finally held at 0.4FFP for the rest duration. The variations of the reference and PWR output power are plotted in Fig. 7 (a). The PSO algorithm trains the NN to supervise the PID controller to track the reference input effectively and smoothly as compared with the PSO-PID method.

The main object of any controller is to filter the error and generate the control input. The control input is fed to the PWR core model to optimize the output to track the reference input. Fig. 7 (b) displays the control rod speed computed by both controllers. The Jacobian values and the performance of the PSO-NN supervisory controller are depicted in Figs. 7 (c) and (d) respectively.

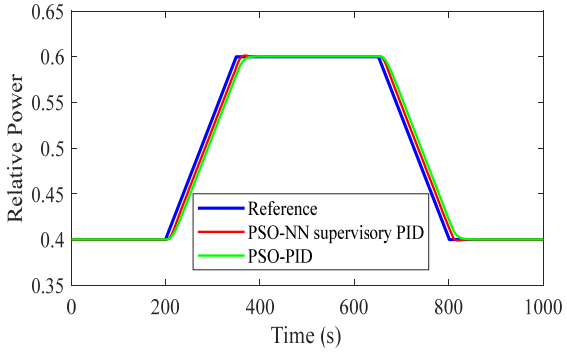

(a) Relative power

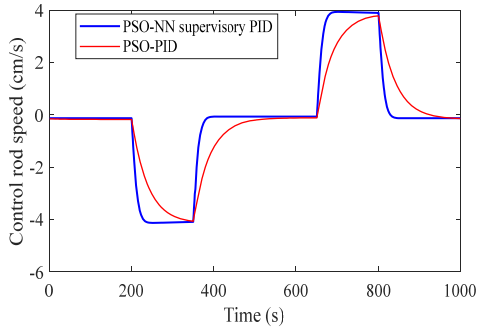

(b) Control input

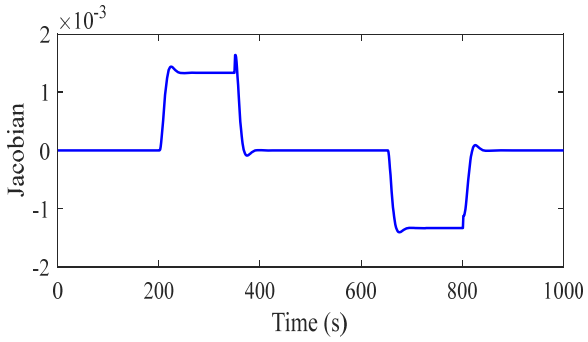

(c) The sensitivity

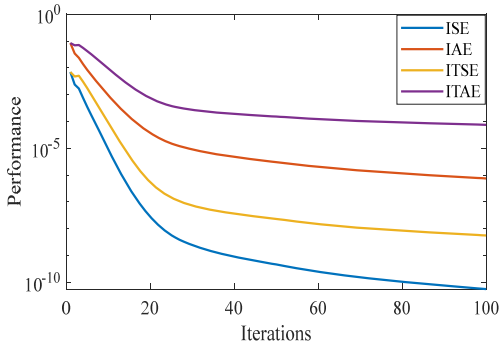

(d) Performance of the controller

Fig. 7 The simulation results

The PWR model shows a frequency nature and can be represented using the Bode diagrams. The Bode plot is used to evaluate the stability in terms of gain and phase. The gain margin (GM), and phase margin (PM) at the crossover frequency are mathematically expressed as;

$$GM = 0 - G \tag{38}$$

$$PM = \phi - (-180^{\circ}) \tag{39}$$

where, G and ϕ are the gain and phase lag respectively.

Fig. 8 shows the Bode plot of the PWR core. The GM, PM, and crossover frequency of the PWR model are 150dB, 73.8°, and 0.346 rad/s respectively. Both GM and PM are positive and confirm the stability of the PWR core model.

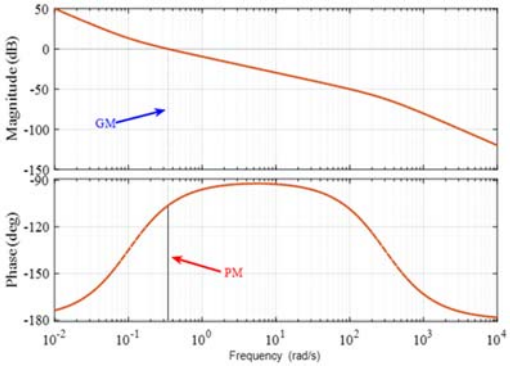

Fig. 8 Bode plot

REFERENCES

[1] R. P. Borase, D. K. Maghade, S. Y. Sondkar, and S. N. Pawar, "A review of PID control, tuning methods and applications," Int. J. Dyn. Control, Jul. 2020, doi: 10.1007/s40435-020-00665-4.

[2] M. Zarei, R. Ghaderi, N. Kojuri, and A. Minuchehr, "Robust PID control of power in lead cooled fast reactors: A direct synthesis framework," Ann. Nucl. Energy, vol. 102, pp. 200–209, Apr. 2017, doi: 10.1016/j.anucene.2016.12.017.

[3] S. M. H. Mousakazemi, N. Ayoobian, and G. R. Ansarifar, "Control of the reactor core power in PWR using optimized PID controller with the real-coded GA," Ann. Nucl. Energy, vol. 118, pp. 107–121, Aug. 2018, doi: 10.1016/j.anucene.2018.03.038.

[4] M. Zarei, "A physically-based PID controller for the power maneuvering of nuclear reactors," Prog. Nucl. Energy, vol. 127, p. 103431, Sep. 2020, doi: 10.1016/j.pnucene.2020.103431.

[5] A. Salehi, O. Safarzadeh, and M. H. Kazemi, "Fractional-order PID control of steam generator water level for nuclear steam supply systems," Nucl. Eng. Des., vol. 342, pp. 45–59, Feb. 2019, doi: 10.1016/j.nucengdes.2018.11.040.

[6] K. Nabeshima, T. Suzudo, T. Ohno, and K. Kudo, "Nuclear reactor monitoring with the combination of neural network and expert system," Math. Comput. Simul., vol. 60, no. 3–5, pp. 233–244, Sep. 2002, doi: 10.1016/S0378-4754(02)00018-6.

[7] M. N. Khajavi, M. B. Menhaj, and A. A. Suratgar, "A neural network controller for load following operation of nuclear reactors," Ann. Nucl. Energy, p. 10, 2002, doi:10.1016/S0306-4549(01)00075-5

[8] J. H. Pérez-Cruz and A. Poznyak, "Automatic startup of nuclear reactors using differential neural networks," IFAC Proc. Vol., vol. 40, no. 20, pp. 112–117, 2007, doi: 10.3182/20071017-3-BR-2923.00019.

[9] H. Shen and J. M. Doster, "Application of a neural network-based feedwater controller to helical steam generators," Nucl. Eng. Des., vol. 239, no. 6, pp. 1056–1065, Jun. 2009, doi: 10.1016/j.nucengdes.2009.02.011.

[10] H. G. Kim, S. H. Chang, and B. H. Lee, "Pressurized Water Reactor Core Parameter Prediction Using an Artificial Neural Network," Nucl. Sci. Eng., vol. 113, no. 1, pp. 70–76, Jan. 1993, doi: 10.13182/NSE93-A23994.

[11] S. O. Starkov and Y. N. Lavrenkov, "Prediction of the moderator temperature field in a heavy water reactor based on a cellular neural network," Nucl. Energy Technol., vol. 3, no. 2, pp. 133–140, Jun. 2017, doi: 10.1016/j.nucet.2017.05.008.

[12] T. V. Santosh, G. Vinod, R. K. Saraf, A. K. Ghosh, and H. S. Kushwaha, "Application of artificial neural networks to nuclear power plant transient diagnosis," Reliab. Eng. Syst. Saf., vol. 92, no. 10, pp. 1468–1472, Oct. 2007, doi: 10.1016/j.ress.2006.10.009.

[13] M. Gomez Fernandez, A. Tokuhiro, K. Welter, and Q. Wu, "Nuclear energy system's behavior and decision-making using machine learning," Nucl. Eng. Des., vol. 324, pp. 27–34, Dec. 2017, doi: 10.1016/j.nucengdes.2017.08.020.

[14] A. Mathew, P. Amudha, and S. Sivakumari, "Deep Learning Techniques: An Overview, in Advanced Machine Learning Technologies and Applications," vol. 1141, A. E. Hassanien, R. Bhatnagar, and A. Darwish, Eds. Singapore: Springer Singapore, 2021, pp. 599–608. doi: 10.1007/978-981-15-3383-9_54.

[15] B. Vasumathi and S. Moorthi, "Implementation of hybrid ANN–PSO algorithm on FPGA for harmonic estimation," Eng. Appl. Artif. Intell., vol. 25, no. 3, pp. 476–483, Apr. 2012, doi: 10.1016/j.engappai.2011.12.005.

[16] P. Pant, Prediction of clad characteristics using ANN and combined PSO-ANN algorithms in laser metal deposition process, Surf. Interfaces, p. 10, 2020.

[17] C. M. Pareek, V. K. Tewari, R. Machavaram, and B. Nare, "Optimizing the seed-cell filling performance of an inclined plate seed metering device using integrated ANN-PSO approach," Artif. Intell. Agric., vol. 5, pp. 1–12, 2021, doi: 10.1016/j.aiia.2020.11.002.

[18] S. Ahmadi, Sh. Abdi, and M. Kakavand, "Maximum power point tracking of a proton exchange membrane fuel cell system using PSO-PID controller," Int. J. Hydrog. Energy, vol. 42, no. 32, pp. 20430–20443, Aug. 2017, doi: 10.1016/j.ijhydene.2017.06.208.

[19] S. M. H. Mousakazemi and N. Ayoobian, "Robust tuned PID controller with PSO based on two-point kinetic model and adaptive disturbance rejection for a PWR-type reactor," Prog. Nucl. Energy, vol. 111, pp. 183–194, Mar. 2019, doi: 10.1016/j.pnucene.2018.11.003.

[20] L. K. Carvalho, Y.-C. Wu, R. Kwong, and S. Lafortune, "Detection and mitigation of classes of attacks in supervisory control systems," Automatica, vol. 97, pp. 121–133, Nov. 2018, doi: 10.1016/j.automatica.2018.07.017.

[21] M. Baranwal and S. Salapaka, "Clustering and supervisory voltage control in power systems," Int. J. Electr. Power Energy Syst., vol. 109, pp. 641–651, Jul. 2019, doi: 10.1016/j.ijepes.2019.02.025.

[22] M. Lotfi, M. B. Menhaj, S. A. Hosseini, and A. S. Shirani, "A design of switching supervisory control based on fuzzy-PID controllers for VVER-1000 pressurizer system with RELAP5 and MATLAB coupling," Ann. Nucl. Energy, vol. 147, p. 107625, Nov. 2020, doi: 10.1016/j.anucene.2020.107625.

[23] Z. Dong, X. Huang, Y. Dong, and Z. Zhang, "Multilayer perception-based reinforcement learning supervisory control of energy systems with application to a nuclear steam supply system," Appl. Energy, vol. 259, p. 114193, Feb. 2020, doi: 10.1016/j.apenergy.2019.114193.

[24] A. Ouaret, H. Lehouche, B. Mendil, and H. Guéguen, "Supervisory control of building heating system with insulation changes using three architectures of neural networks," J. Frankl. Inst., vol. 357, no. 18, pp. 13362–13385, Dec. 2020, doi: 10.1016/j.jfranklin.2020.09.027.

[25] T. Zhang and K. E. Holbert, "Frequency Domain Comparison of Multi-lump and Distributed Parameter Models for Pressurized Water Reactor Cores," Am. J. Energy Res., vol. 1, no. 1, pp. 17–24, Feb. 2013, doi: 10.12691/ajer-1-1-3.

[26] G. Wang, J. Wu, B. Zeng, Z. Xu, W. Wu, and X. Ma, "State-Space Model Predictive Control Method for Core Power Control in Pressurized Water Reactor Nuclear Power Stations," Nucl. Eng. Technol., vol. 49, no. 1, pp. 134–140, Feb. 2017, doi: 10.1016/j.net.2016.07.008.

[27] S. M. H. Mousakazemi, "Control of a PWR nuclear reactor core power using scheduled PID controller with GA, based on two-point kinetics model and adaptive disturbance rejection system," Ann. Nucl. Energy, vol. 129, pp. 487–502, Jul. 2019, doi: 10.1016/j.anucene.2019.02.019.

[28] O. Ahmed, L. Hocine, M. Boubekeur, F. Siham, and G. Herve, "Supervisory control of a building heating system based on radial basis function neural networks," in 2017 5th International Conference on Electrical Engineering - Boumerdes (ICEE-B), Boumerdes, Oct. 2017, pp. 1–6. doi: 10.1109/ICEE-B.2017.8192182.

[29] S. Khatir, S. Tiachacht, C.-L. Thanh, T. Q. Bui, and M. Abdel Wahab, "Damage assessment in composite laminates using ANN-PSO-IGA and Cornwell indicator," Compos. Struct., vol. 230, p. 111509, Dec. 2019, doi: 10.1016/j.compstruct.2019.111509.

[30] W. J. Blackwell, "Neural network Jacobian analysis for high-resolution profiling of the atmosphere," EURASIP J. Adv. Signal Process., vol. 2012, no. 1, p. 71, Dec. 2012, doi: 10.1186/1687-6180-2012-71.